

Prototyping of Radial and Thrust Air Bearing for Micro Gas Turbine

Susumu KITAZAWA, Shigehiko KANEKO and Tastuo WATANABE

Department of Mechanical Engineering
the University of Tokyo
7-3-1 Hongo, Bunkyo-ku, Tokyo 113-8656, JAPAN
Phone: +81-3-5841-6430, FAX: +81-3-5689-8054, E-mail: kitazawa@fiv.t.u-tokyo.ac.jp

ABSTRACT

Self-acting micro air bearings are demanded for developing high performance, maintenance free micro gas turbines. In this study, we designed and manufactured both radial and thrust foil bearings and developed two types of apparatuses for testing the performance of these bearings. These bearings were tested for both vertical and horizontal rotors by utilizing rotors from commercially available turbochargers.

The apparatus for testing a vertical rotor consists of gas lubricated foil bearings for a radial bearing and an externally pressurized gas bearing with multiple air supply holes for a thrust bearing. The other apparatus for testing a horizontal rotor consists of gas lubricated foil bearings for both radial and thrust bearings. We measured rotational speed and vibrations in the radial and axial directions.

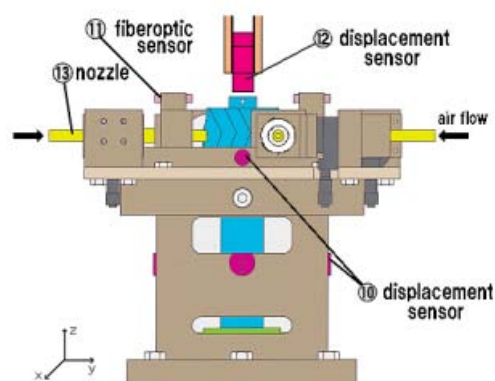
INTRODUCTON

In recent years, an easily maintainable micro gas turbine (MGT) of 100kW or less is drawing close attention as a power generator equipped with cogeneration features. Aerodynamic foil bearings are considered to be the best candidates for the MGT due to its ease of maintenance.

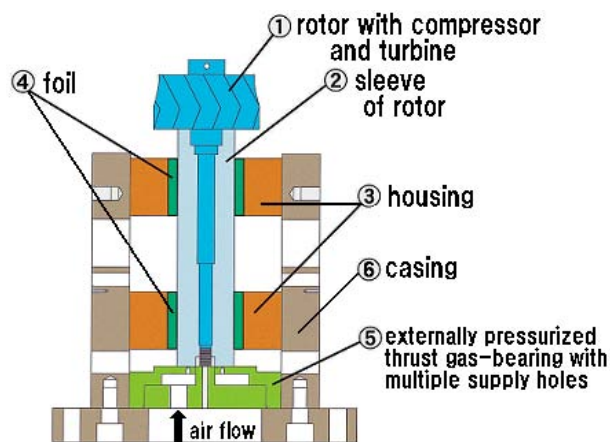
In this study, we designed and manufactured foil bearings for a small rotor (diameter of 20~30mm), in which its characteristics and potential problems were determined. Moreover, we manufactured two experimental apparatuses for the vertical and horizontal rotors where an aerostatic bearing and aerodynamic foil bearing were adopted as a thrust bearing, respectively. The foil bearing used in this study was composed of a phosphor bronze foil given some hemisphere-like projections and a housing.

APPARATUS OF VERTICAL TYPE AND EXPERIMENTAL PROCEDURES

The experimental apparatus of vertical type is shown in Fig.1(a) and (b).



(a) Front view



overall height	200 mm
diameter of casing	120 mm

(b) Cross sectional view

Fig.1 Experimental apparatus of vertical type

Construction and Dimensions of Radial Bearings

The layout of the manufactured radial foil bearing is shown in Fig.2. This bearing is composed of two elements; i.e. a housing and a foil with projections of hemisphere on one side in the adequate interval. The foil is made from a phosphor bronze plate of 0.1mm in thickness, 30mm in width, 296mm in length, and has 160 hemispherical projections whose height is 0.2mm (Fig.3). When we first assembled the radial foil bearing, the plate was bent from the edge in the position of 3mm, and it was embedded in the attaching portion of the housing. Then, the foil was wound spirally and fixed with the housing. Due to the rotating shaft, a wedge like space is created between the shaft and the bearing surface. From this opening, the air stream velocity rises, causing the shaft to slightly levitate. This levitation by the shaft is known as bearing action. The housing is made of brass and the inside diameter of the housing is 31.44mm. The bearing clearance is represented as C and is described by the equation as follows;

$$C = (D - d) / 2 - 2h - 3t \tag{1}$$

where C , D , d , h and t are radial clearance, inner diameter of housing, diameter of rotor, height of projections and thickness of the foil, respectively. The bearing radial clearance between axial surface and bearing surface is $20 \mu m$, because the foil is triply wounded.

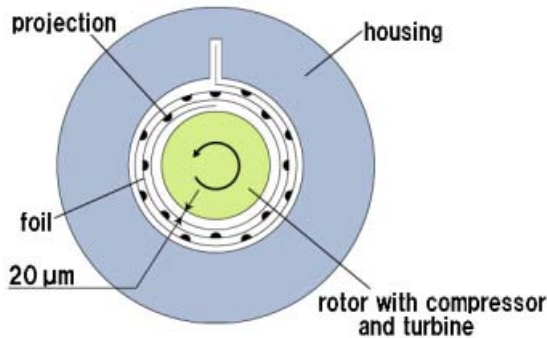


Fig.2 Schematic view of foil bearing

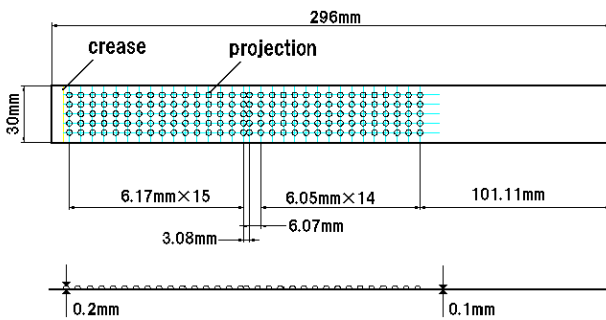


Fig.3 Dimensions of foil and projections

Production Process of Foil

The foil used here was manufactured by wet etching and the press (Fig.4) was used in the designing and processing of projections. The side of the press is set with the x-y stage as shown in Fig.4. The structure of the dice is shown in Fig.6. On the top die, a larger hole than the diameter of the steel

ball was drilled in the center considering the thickness of the foil. On the bottom die, a “V” shaped groove was made by Electrical Discharge Machining (EDM). The steel ball was placed in the groove as shown in Fig.6.

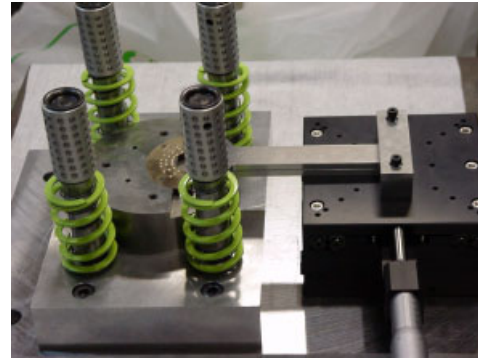


Fig.4 Picture of the press

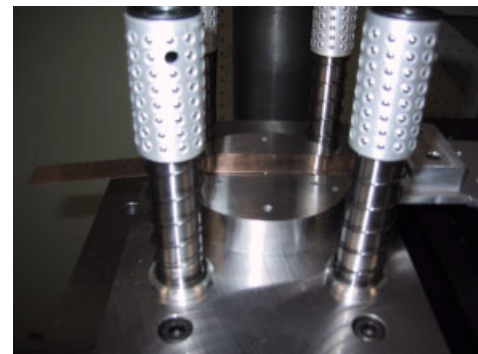


Fig.5 Picture of the press construction part

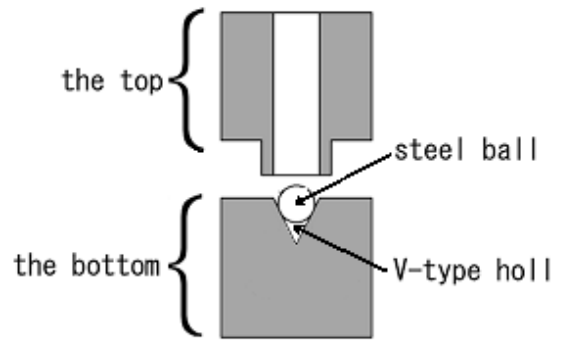


Fig.6 Schematic view of the dice

Construction and Dimensions of Rotor

The rotor used in this experimental apparatus is composed of two elements which are the shaft with turbine (Fig.1(b)①) and the sleeve(Fig.1(b)②). The material used for the sleeve was carbon steel, the surface of the shaft has a ceramic coating, and the bottom is coated with hard chrome. The sleeve was fixed with the shaft by inserting it under pressure.

Major dimensions of the rotor are shaft diameter 30mm, length 161mm and weight 0.9kg. The rotor is equipped with a through hole in the upper part of the turbine for measuring rotational speed.

Construction and Dimensions of Thrust Bearing

In this experimental apparatus, an aerostatic bearing was adopted for a thrust bearing as is shown in Fig.1(b)⑤. In designing the gas bearing, it is necessary to grasp bearing performances such as load capacity, rigidity, flow rate, and stability of the bearing, which are controlled by the pressure distribution of the gas in the bearing clearance. The pressure distribution can be evaluated based on Navier-Stokes' equation, the continuity equation, the ideal gas law and the energy equation.

Generally, Reynolds' equation is obtained assuming that the fluid is Newtonian fluid, laminar flow, neglecting body forces, and that the bearing clearance is much smaller than other dimension, and so on.

$$\frac{\partial}{\partial x} \left(\frac{\rho h^3}{\mu} \frac{\partial p}{\partial x} \right) + \frac{\partial}{\partial y} \left(\frac{\rho h^3}{\mu} \frac{\partial p}{\partial y} \right) = 6 \left\{ U_x \frac{\partial(\rho h)}{\partial x} + U_y \frac{\partial(\rho h)}{\partial y} \right\} \quad (2)$$

Using this equation, the performance calculation of an externally pressurized gas bearing with multiple air supply holes as shown in Fig.7, is carried out, and then, dimensions are decided from the bearing characteristics.

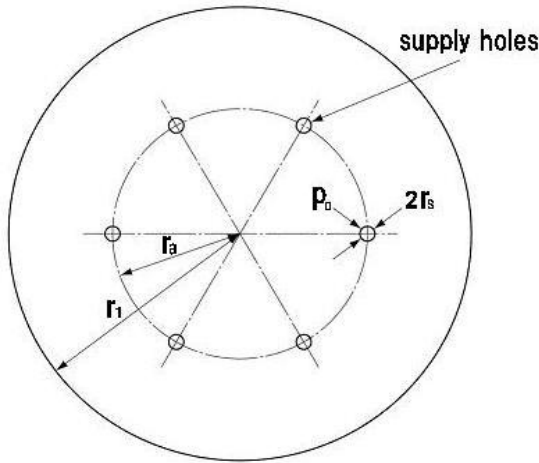


Fig.7 Schematic view of externally pressurized gas bearing with multiple supply holes

Major dimensions of the aerostatic thrust bearing can be decided by the condition when the maximum load capacity is attained. We then obtained the bearing diameter $r_1 = 15\text{mm}$ from the fact that the diameter of the shaft is 30mm , the number of air supply holes $k = 8$, the radius of air supply holes $r_s = 0.15\text{mm}$, and the location of air supply holes $r_a = 9\text{mm}$.

The load capacity W of this bearing is represented as follows;

$$W = \pi r_1^2 (p_0 - p_a) F_w \quad (3)$$

$$= 2.3 \text{ [kg]}$$

$$\left(\begin{array}{l} F_w : \text{dimensionless load capacity} \\ p_0 = 2p_a : \text{pressure at air supply hole exit} \\ p_a : \text{atmospheric pressure} \end{array} \right)$$

Evaluating the load capacity of the thrust bearing, we have to consider the weight of a rotating shaft together with aerodynamic thrust force induced by turbine blades. However, we estimated that the aerodynamic thrust force is small enough. Since the range of the air pressure level available in our air supply system is $0 \sim 6 P_a$, we put P_0 twice as P_a (atmospheric pressure) in Eq.(3). Then, we obtained the load capacity $W = 2.3\text{kg}$, which is larger than the weight of the rotor used in this experimental apparatus, 0.9kg .

In what follows, the construction of the aerostatic thrust bearing will be explained. This bearing consists of two elements, which are the part with air supply holes and its counter pair. Here, we will explain how we machined air supply holes. As shown in Fig.8, first, a hole of the 3mm depth was drilled using the drill of the 2mm diameter, and 1mm depth was drilled through using the drill of 0.3mm which was the diameter of the air supply hole. In the latter parts as shown in Fig.1(b)⑤, there is a hole of 3mm diameter in the center so that the supplied air from an air supply hole can be released in the atmosphere. The materials of both parts are made of brass, and both parts were adhesively fixed.

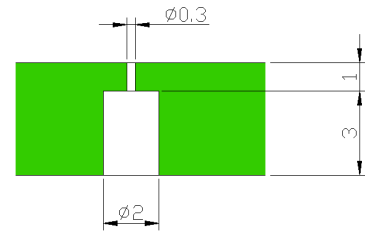


Fig.8 Air supply hole

Experimental Procedure

First, we floated the rotor by opening the pressure regulating valve to control the supply flow rate. Then, the rotational speed was controlled by adjusting the supply air quantity to the turbine by switching the pressure regulating valve connected to the nozzle.

Optical fiber sensors were used to make measurements for the rotational speed. For measurements of displacement in the x-y direction, eddy current type displacement sensors are installed at the positions corresponding to top and bottom of the rotor. The displacement in the z direction was measured at the position of the upper turbine. All the signals from these displacements sensors were recorded with the rotational speed.

APPARATUS OF HORIZONTAL TYPE AND EXPERIMENTAL PROCEDURES

Aiming at removing auxiliary equipments such as the compressor for air supply and pressure regulating valves used for aerostatic bearing, we designed and manufactured a horizontally positioned experimental apparatus where the rotor is fully supported by aerodynamic foil bearings. The experimental apparatus is shown in Fig.9.

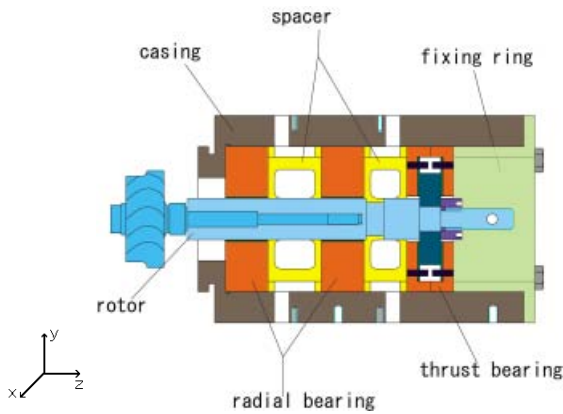


Fig.9 Experimental apparatus

Construction and Dimensions of Radial Bearings

Similar to the vertically positioned apparatus rotor, the foils used are phosphor bronze plates of 0.1mm thickness, 202mm length, 20mm width, and with hemispherical projections. The housing made of brass has an inside diameter of 21.44mm, which was designed so that the bearing radial clearance would be $20 \mu\text{m}$.

Construction and Dimensions of Rotor

The structure of the rotor used in this experiment is shown in Fig.10. The rotating shaft consists of the following four parts, the rotor with turbine, a sleeve, a thrust disk, and a nut for fixing the thrust disk to the rotor. The martensitic stainless steel was used for the sleeve, and the surface is coated by ceramic. At the right end of the rotating shaft, a reverse thread was cut in order to fix the thrust disk, and a through hole was drilled for measuring the rotational speed. The sleeve was inserted under pressure and fixed with the shaft as is the case with vertical rotor.

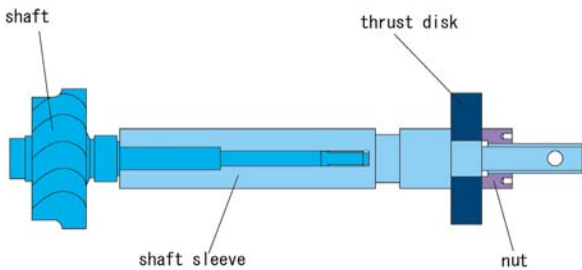


Fig.10 Schematic view of rotor

Construction and Dimensions of Thrust Bearings

The structure of the thrust foil bearing is shown in Fig.11. The thrust bearings are composed of two sets of piled three phosphor bronze annular plates on the housing, which are called a bottom foil, a bump foil and a top foil in order from the bottom. Hemispherical projections were added to the bottom foil and the bump foil with a specific pattern, and these were piled and fixed by pins. Both the bottom foil and the bump foil have four groups of projections that are 90 degree apart. The bump foil is shifted 45 degrees with respect to the bottom foil when stacked. The bearing action was obtained when the dynamic pressure was generated by the bending motion of the foil between the thrust disk and the top foil when the rotor rotates, where the bearing clearance between the thrust disk and the top foil is $50 \mu\text{m}$.

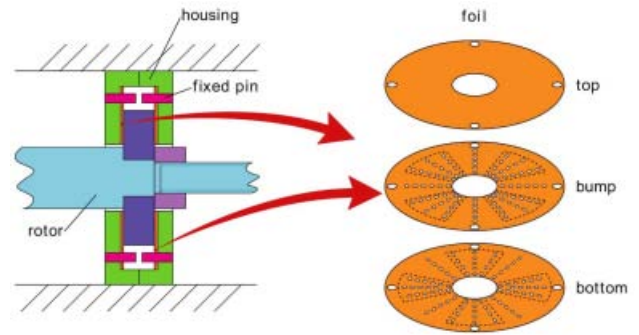


Fig.11 Schematic view of thrust gas bearing

Experimental Procedures

Actual experimental apparatus as shown in Fig.12 installed the cover, the flange and various measuring instruments. By sending the air to the turbine blade by a fan and blower, the rotor starts to rotate. The displacement in the x-y direction was measured at the positions corresponding to top and bottom of rotating shaft by eddy current type displacement sensors, and the displacement of z direction was measured at the shaft edge. The rotational speed was detected by the optical fiber sensor, and was recorded together with the displacements of each direction.

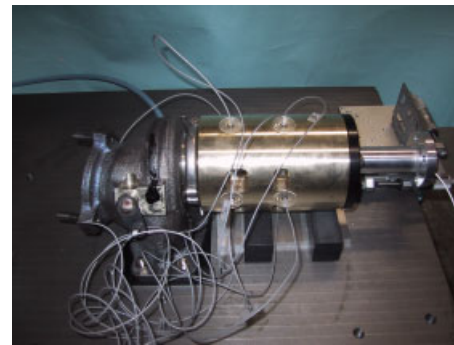


Fig.12 Picture of the experimental apparatus

EXPERIMENTAL RESULT AND CONSIDERATION ON VERTICAL TYPE APPARATUS

In Fig.13, the oscillatory waveform when the rotational speed is around 10,000rpm (168Hz) is shown. The relation between rotational speed and the pressure of air supplied to the turbine is shown in Fig.14. From the recorded data with the displacements in x-y direction in Fig.13, the amplitude due to vibrations of the rotating shaft is found to be $7\sim 10 \mu\text{m}$, hence, it is shown that the amplitude is smaller than the bearing clearance ($20 \mu\text{m}$), which means the rotor does not contact with the bearing surface. From the displacement in the z direction, the rotating shaft is floated in the position of $12 \mu\text{m}$ and vibrates with the amplitude of $3 \mu\text{m}$, and it can be confirmed that the shaft rotates without contacting with the thrust bearing. Additionally, there is higher frequency around 2,000Hz in the x-y rotor displacements in Fig.13. This high frequency seems to come from the blade passing frequency. Since the blade number is 11, then 11 times rotational frequency 168 Hz makes about 1850Hz.

From Fig.14, a gentle rise in rotational speed in the low speed area is not seen but the rotational speed suddenly rises

at a specific turbine air pressure corresponding to about 6,500rpm. This shows that the rotor contacts with the bearing at the beginning, proving that the starting torque is large. In addition, it can be proved that rotational speed is proportion to flow rate.

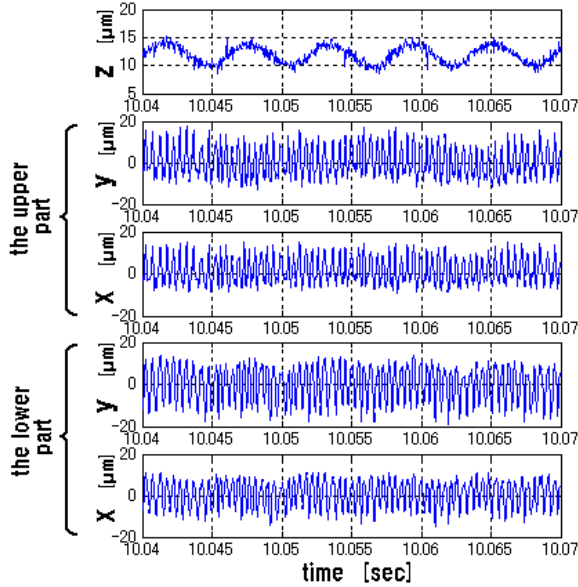


Fig.13 Rotor displacement (at 10,000rpm)

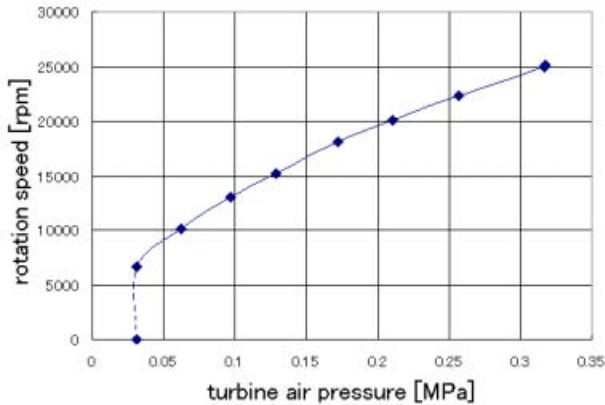


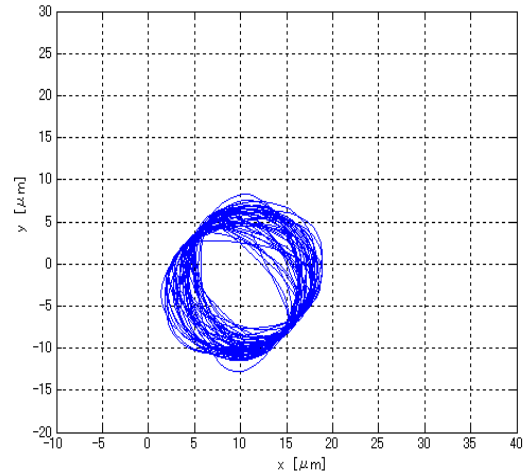
Fig.14 Relation between rotational speed and turbine air pressure

EXPERIMENTAL RESULT AND CONSIDERATION ON HORIZONTAL TYPE APPARATUS

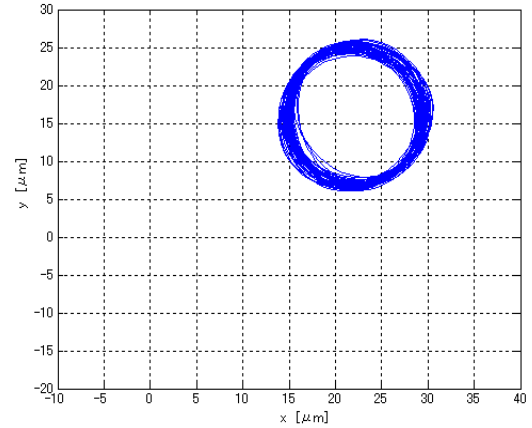
The data measured at 25,000rpm is shown in Fig.15(a) and (b). Fig.15 shows Lissajous figures of the x-y direction at the upper and the lower parts, which shows that the amplitude of whirling motion is about 7 μ m. Fig.16 shows frequency characteristics of the x, y, z displacement, and a large peak is found to exist at 420Hz, which is the frequency equal to the rotational frequency, i.e., the component which synchronizes with the rotational frequency. Since the radial clearance is 20 μ m, the shaft is therefore proven to rotate without contacting with the radial bearings.

Contrary to x- direction, in the z direction, a small peak also can be found at 850Hz which corresponds to higher harmonics of the rotational frequency. This peak suggests

contact phenomenon of the top foil against the thrust disk. In Fig.17, the damaged top foil after several times on-off experiments is shown and the traces of damage can be found on the surface.



(a) the upper part (at 25,000rpm)



(b) the lower part (at 25,000rpm)

Fig.15 Lissajous figure

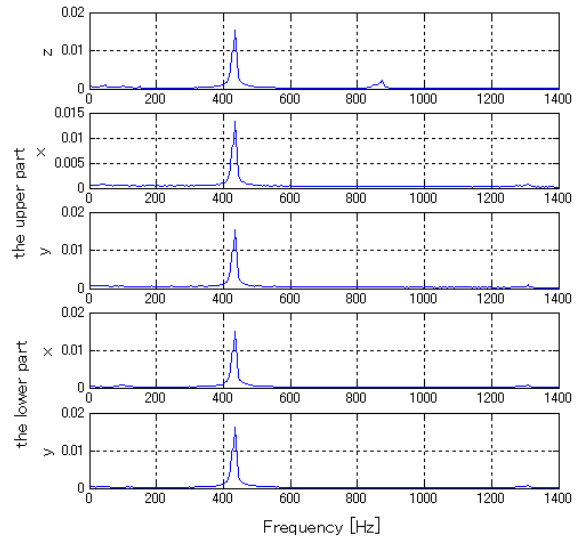


Fig.16 Frequency characteristics of rotor displacement (at 25,000rpm)



Fig.17 Picture of damaged top foil

In Fig.18 and 19, the data from the start to 30,000rpm are shown. Fig.18 shows rotational speed rise in the starting stage, and Fig.19 shows vibration of the rotor in x, y, z direction. From Fig.18, the shaft begins to rotate after about 3 seconds, and it reaches 30,000rpm in 14 seconds. From Fig.19, the amplitude in the x-y direction once increases in 4 seconds, but until the rotational speed reaches 30,000rpm, the amplitude is settled at $5\ \mu\text{m}$, which is smaller than the bearing clearance ($20\ \mu\text{m}$).

In addition, we can see the difference of vibrational amplitudes between the data of Fig.15 and those of Fig.19. This is because Fig.15 shows the data at constant rotational speed (25,000rpm), while Fig.19 shows rotor displacements in the transition phase from the start to 30,000rpm.

CONCLUSION

In this study, we successfully designed and manufactured foil bearings for the rotor with a small diameter. These bearings were examined with performance and vibration characteristics. From the test result, it becomes clear that the radial foil bearings produced could support the shafts of 30mm and 20mm diameters.

The surfaces of the rotor and the radial bearings did not deteriorate even if the tests were repeatedly carried out. Yet on the thrust bearing, the trace which shows contact phenomenon of top foil against thrust disk can be found on their surfaces.

In order to contribute to propose design methods of foil bearings, further experiments and analyses are necessary.

ACKNOWLEDGEMENT

This work was carried out as part of NEDO Project -"Practical Application and Technological Development of Button Type of Gas Generator".

In this study, we express our appreciation to Prof. Shigeka Yoshimoto (Tokyo University of Science) who taught us the technique on the bearing design and advised us on our study.

We would like to thank Mr. Yu Watanabe at the University of Tokyo, whose work made this paper possible. We would also thank Mr. Yohei Jorge Matsumoto for his contribution on English translation.

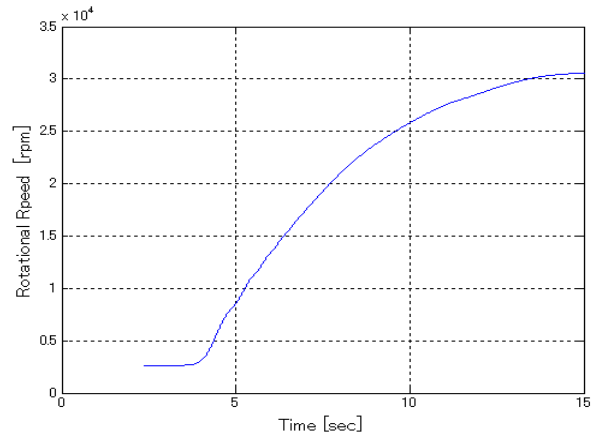


Fig.18 Rotational speed in the starting stage

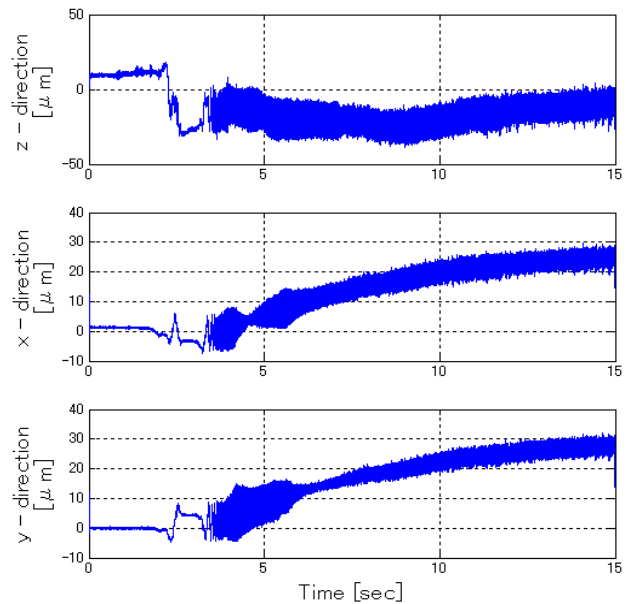


Fig.19 Rotor displacement in the starting stage

REFERENCES

- Heshmat. H, 2000, "Operation of Foil Bearings Beyond the Bending Critical Mode," ASME Journal of Tribology, Vol.122, pp.192~198
- Heshmat. H, 2000, "Analysis of Gas Lubricated Foil Thrust Bearing Using Coupled Finite Element and Finite Difference Methods", ASME Journal of Tribology, Vol.122, pp.199~204
- Hayashi. K and Hirasata. K, 1994, "Developments of Aerodynamic Foil Bearings for Small High-speed Rotor," Proc. of 21st Leeds-Lyon Symp. , pp.291~299
- Haruo Mori and Hiroshi YABE, 1964, "Analysis of Externally Pressurized Circular Thrust Gas-Bearing with Multiple Supply Holes," Junkatu, Vol.9, pp.35~41